Research Article | Vol. 27, No. 3 | 4 Feb 2019 | OPTICS EXPRESS 2101
Optics EXPRESS

Second harmonic generation of femtosecond laser written depressed cladding waveguides in periodically poled MgO:$LiTaO_3$ crystal

LEI WANG,[1,*] XINTONG ZHANG,[1] LINGQI LI,[1] QINGMING LU,[2] CAROLINA ROMERO,[3] JAVIER R. VÁZQUEZ DE ALDANA,[3] AND FENG CHEN[1]

[1]*School of Physics, State Key Laboratory of Crystal Materials, Shandong University, Jinan, 250100, China*
[2]*School of Chemistry and Chemical Engineering, Shandong University, Jinan, 250100, China*
[3]*Grupo de Investigación en Aplicaciones del Láser y Fotónica, Departamento de Física Aplicada, University of Salamanca, Salamanca, 37008, Spain*
**leiwangsdu@sdu.edu.cn*

Abstract: We report on the fabrication of depressed cladding waveguides in periodically poled MgO doped $LiTaO_3$ by using low-repetition-rate femtosecond laser writing, and their use for guided-wave second harmonic generation (SHG). The cladding waveguides exhibit different guiding performance along the extraordinary and ordinary polarizations. The temperature-dependent quasi-phase-matching (QPM) is realized to obtain SHG in the depressed cladding waveguides. The results show that the QPM temperature was dependent on the poling period and on the features of the cladding waveguides. The highest nonlinear conversion efficiency ($0.74\%W^{-1}cm^{-2}$) was found in the waveguide fabricated with large scanning velocity (0.75 mm/s) and small radius (15 μm).

1. Introduction

Ferroelectric oxide monocrystalline, such as lithium niobate ($LiNbO_3$) [1,2], lithium tantalate ($LiTaO_3$ or LT) [3–5] and $KTiOPO_4$ (KTP) [6,7], are becoming increasingly important in the fields of nonlinear photon generation and manipulation due to their high nonlinear conversion efficiency and broad light spectrum acceptance. Optical waveguides are one of the key components in integrated circuits. Its most unique property is that high light intensity within a long interaction length can be realized because of the elimination of diffraction inside the waveguide [8,9], which is desired in nonlinear interaction process. Several kinds of techniques, such as ion exchange [2–4], metal thermal diffusion [9–12] and ion irradiation [13,14] have been used to produce effective optical waveguides in these ferroelectric oxide single crystals. Femtosecond laser writing (FLW) has been investigated as a powerful tool not only for material machining [15–17] but also for the subtle optical modification of materials [18]. This method has been applied to a wide range of passive and active media to create integrated devices such as waveguides [19–32], directional couplers [35,36], Bragg gratings [37,38] and waveguide lasers [39–43]. The femtosecond pulses could even be employed to control/reverse the ferroelectric micro-domains in $LiNbO_3$ [44–46] and barium calcium titanate crystal [47].

Despite of its lower second order nonlinear optical coefficient (d_{33}) compared to $LiNbO_3$, $LiTaO_3$ crystal possess higher optical damage threshold [48,49] which implies that $LiTaO_3$ devices have larger potential to handling high power light. The magnesium oxide (MgO) could be doped during the crystal growth process to improve the optical damage threshold further. It should also be noted that $LiTaO_3$ is transparent to 280nm and is therefore more suitable than $LiNbO_3$ for nonlinear optical interactions in the mid UV, which is transparent to 330nm [50]. However, the main obstacle for fabrication of domain grating with high spatial resolution and fine pitch is the excessive polarization electric field, which is induced by the

#347714 https://doi.org/10.1364/OE.27.002101
Journal © 2019 Received 11 Oct 2018; revised 8 Dec 2018; accepted 13 Dec 2018; published 24 Jan 2019

Optics EXPRESS

inherent defects of $LiTaO_3$ crystal, such as lithium vacancies and anti-tantalum at room temperature. The improvement of Li/Ta from congruent $LiTaO_3$ to near stoichiometric $LiTaO_3$ (SLT) could reduce the coercive field further [51,52]. Periodically poled nonlinear domain gratings with finer footprint or larger aperture can be fabricated in SLT. Nowadays, periodically poled MgO doped SLT (MgO:PPSLT) with complicated domain gratings, such as fan-out or two dimensional patterns have already been available [53,54]. Recently FLW depressed cladding waveguide has been formed in various materials [28–30]. This type of waveguide consists an array of written tracks which act as the cladding layer. Light can be confined in the core region to propagate. The properties of the core region can be well preserved. Chen *et al*. have fabricated cladding waveguides inside $LiTaO_3$ [33]. The linear optical properties including propagation loss and polarized behaviors have been demonstrated. Mcmillen *et al*. reported the FLW waveguides in $LiTaO_3$ using different pulse energies and translation speeds [34]. Second harmonic microscopy was also implemented to acquire the nonlinear optical properties in the irradiated region. For $LiNbO_3$ crystal, there have been many reports about the FLW waveguides [21–29]. SHG with considerable conversion efficiencies have been achieved by birefringence PM [23] or QPM techniques [24,26–28]. For $LiTaO_3$, SHG at infrared waveband has been demonstrated by the reverse proton exchange method [4]. However, no direct frequency doubling observation was reported in FLW $LiTaO_3$ waveguides.

In this work, we report on the fabrication of cladding waveguide structures in MgO:PPSLT with nearly circular cross sections. The temperature dependent SHG at pump wavelength of 1064nm was investigated to show the nonlinear properties of the present waveguide structures.

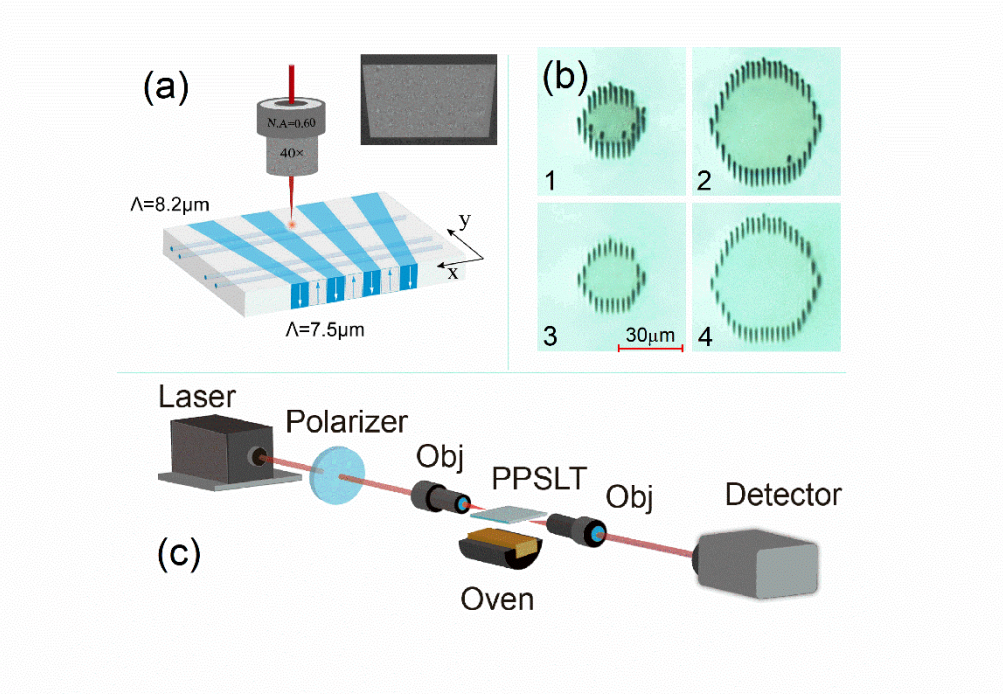

Fig. 1. (a) The schematic illustration of fan-out pattern on MgO:PPSLT sample and the FLW process. (b) The microscopic picture of waveguide WG1-WG4. (c) The setup of the end face coupling measurements.

Optics EXPRESS

2. Theory and experiments

The *z*-cut PPSLT sample doped with 1% MgO consists of a fan-out domain-inverted grating with dimension of 11 × 7 × 0.5 mm^3. Figure 1(a) shows the top view of the fan-out pattern. The grating periods of the waveguide channel smoothly varied from 7.5 to 8.2 μm. The designed phase matching SHG wavelength is from 522 nm to 536 nm around 50°C. According to the theory of quasi-phase-matching (QPM), the period of domain inverted region for QPM in SHG process is given by [55]:

$$\Lambda_0 = \lambda/2(n_{2\omega} - n_{\omega}) \tag{1}$$

where $n_{2\omega}$ and n_{ω} denote the refractive index of SHG and pump waves. At a specific temperature, different pump wavelength corresponds to different periods of inverted domain. Because of the temperature dependence of the refractive index of $LiTaO_3$ crystal [56,57], the phase mismatch between the two interacting waves in the zero order QPM process can be expressed by:

$$\Delta = \frac{4\pi}{\lambda_{\omega}}[n_{2\omega}(T) - n_{\omega}(T)] - \frac{2\pi}{\Lambda_0} \tag{2}$$

where T is the temperature of the crystal, λ is the wavelength of the pump light. The best conversion efficiency (Δ = 0) can be reached at different temperatures which correspond to different grating periods. The domain periods versus the pump wavelength at different temperatures are also calculated according to the Sellmeier relations presented in former investigations [57]. The results are depicted in Fig. 2(a). It is found that for a certain wavelength the QPM period reduces if the temperature of the sample increases. Figure 2(b) shows the QPM period versus the temperature under the pump wavelength of 1064 nm (black line).

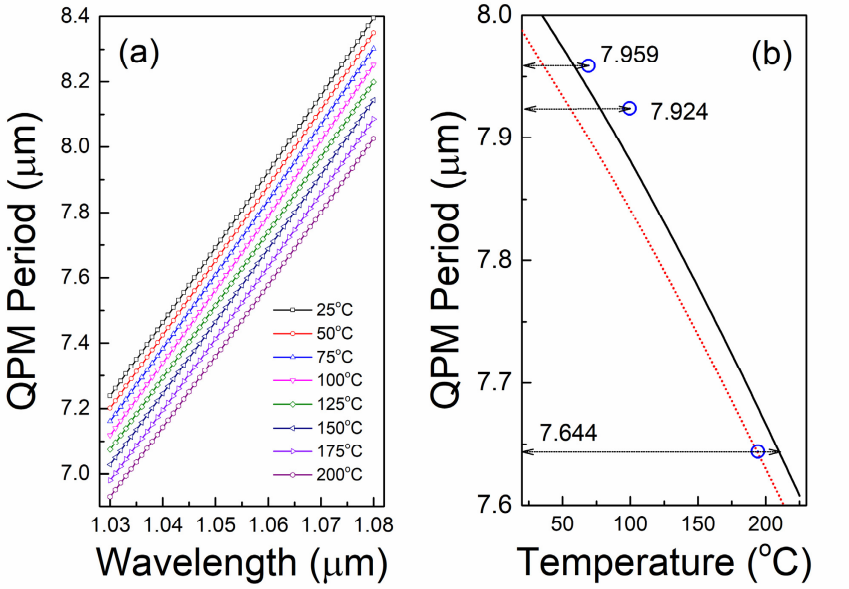

Fig. 2. (a) The QPM period (μm) of MgO doped SLT bulk versus the wavelength at different temperatures. Different lines present different temperatures. (b) Black line, the QPM period (μm) at wavelength of 1064 nm versus different temperature. Red line, the calculated QPM period of WG3 cladding waveguide versus temperature. The three blue circles denote the QPM temperatures of the three cladding waveguides (WG1-WG3).

Optics EXPRESS

During the FLW process, an amplified Ti:Sapphire laser emitted a linearly polarized pulsed beam with duration of 120 fs (central wavelength of 795nm, repetition rate of 1 kHz). The laser beam was focused below the upper surface (11 × 7 mm^2) of the sample with a 40 × microscope objective (N.A. = 0.6). The energy of the incident laser pulse was set to be 0.28 μJ approximately. The sample was placed on a XYZ micro-position stage, while the constant motion velocity was set to be 0.5 mm/s or 0.75 mm/s along the *y*-axis. Tracks were inscribed at different depths with a lateral parallel separation of 3 μm between adjacent ones. The central point of the cladding waveguides are 200 μm beneath the surface. Four oblate circular cross-sectional cladding waveguides named WG1 to WG4 with different radius were fabricated then, as indicated in Fig. 1(b). Table 1 shows the fabrication details of the four waveguides. The poling periods corresponding to the four waveguides are also included.

Table 1. Fabrication details of WG1-WG4

No.	Scan Velocity (mm/S)	Radius (μm)	QPM period (μm)	T_{QPM} (bulk)	T_{QPM} (experimental)
WG1	0.5	15	7.959	57.3 °C	69.1 °C
WG2	0.5	25	7.924	77.5 °C	99.5 °C
WG3	0.75	15	7.644	208.8 °C	194.3 °C
WG4	0.75	25	7.608	225 °C	no data

The second harmonic generation effect together with the insertion loss and beam guidance were investigated with an end-face coupling arrangement. As indicated in Fig. 1(c), the incident light at 1064 nm was generated from a CW solid state laser. A $\lambda/2$ waveplate was employed to adjust the polarization direction of incident light. A 10 × microscope objective lens (N.A. = 0.25) was used as the input coupler between the incident light and the sample, while the output light beam was coupled out of the crystal by another 20 × microscope objective lens (N.A. = 0.40). During the frequency doubling measurements, an Oven (PV10, Covesion Ltd) was utilized for temperature tuning. The temperature range of the oven was 50 °C-200 °C. The polarization of pump light was set to be parallel to *z*-axis of the sample (TM polarization, n_e index) to utilize the d_{33} coefficient.

3. Results and discussion

In order to figure out the angular dependence of the guidance, measurements of the insertion loss as a function of the input polarization direction were carried out at wavelength of 1064nm. Figure 3 depicts all-angle insertion loss measurement of WG1-WG4. It is evident that as the polarization angle varies from 0° to 360°, the insertion loss was not constant. Notably, the minimum insertion loss is achieved when the polarization angles are 0°and 180°, which we will refer to as TM polarization. If the Fresnel Reflection loss of both waveguide facets (about 1.2dB) were offset, we get a minimum propagation loss of 2.1dB/cm at TM polarization. It is believed that the defects in the crystalline lattice may have a significant influence on the optical properties of $LiTaO_3$. During the FLW process, both n_o and n_e in the irradiated region decreased due to the lattice-breakdown effect. Nevertheless, this cannot explain the present polarization dependent transmission behavior in the waveguide core region. It is believed that the Li ion out-diffusion could increase the n_e index of $LiNbO_3$ crystal which has structure similar to $LiTaO_3$ crystal [21]. UV absorption induced Li ion out-diffusion has been demonstrated to enhance the n_e index in $LiNbO_3$ crystal and thus form the channel waveguide structure [58,59]. In the present case of FLW process at 1 kHz repetition rates, we can estimate the Li ion out-diffusion distance according to [22]. Considering the pulse duration of 120 fs, the cold-down time for the crystal lattice should be in the range of tens of μs. The out-diffusion distance of Li ions should be about several nanometers. Therefore the influence of Li ion out-diffusion can be ruled out for the waveguide formation. Another mechanism for the index perturbation is the inner stress induced by the femtosecond laser inscription, which may have a significant influence on the optical properties of SLT crystal. The inner stress induced guiding structures have been demonstrated in $LiNbO_3$ crystals, which has similar symmetry to $LiTaO_3$ in their elastic and elasto-optic tensors [22].

Optics EXPRESS

During the FLW process, stress is induced in the region surrounding the laser focus. At the sides of the laser induced tracks, the index change of TM polarization (n_e) is positive while the index change of TE (n_o) is negative. Therefore, the change of n_e in the core region is positive and the change of n_o is negative. For waveguide mode in TE polarization, the propagating light will cross the surrounding tracks and leak into the surrounding substrate. This is the so-called tunneling effect. As a result, the TE polarized mode will suffer a higher propagation loss.

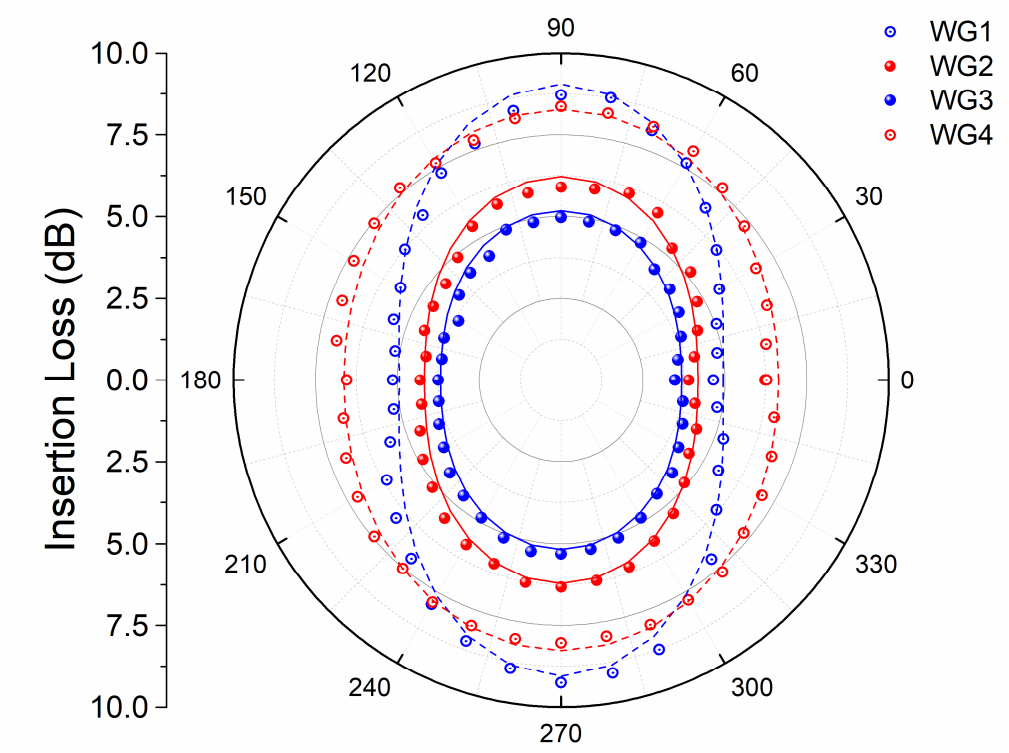

Fig. 3. The angular dependence of output power (transmission) of WG1-WG4 waveguides at wavelength 1064 nm.

We investigated the SHG effect of the four cladding waveguides by tuning the temperature of the sample. All the following SHG measurements were performed preserving the maximum output of the pump light at the rear face of the waveguides. If we assume that the second order nonlinear coefficients are uniform all over the guiding region, the SHG conversion efficiency ($W^{-1}\cdot cm^{-2}$) in a waveguide is given by [4]:

$$\eta = \frac{P_{SHG}}{(P_{pump}\cdot L)^2} = \frac{8\pi^2 d_{QPM}^2}{c\varepsilon_0 n_\omega^2 n_{2\omega}\lambda_\omega^2 A_{eff}} \tag{3}$$

where d_{QPM} is the effective nonlinear coefficient, A_{eff} is the effective nonlinear interaction area which can be calculated by the following overlap integral.

$$A_{eff} = [\iint E_2^{Nor} E_1^{Nor} E_2^{Nor} dxdy]^{-2} \tag{4}$$

E_1^{Nor} and E_2^{Nor} is the normalized field profiles of the pump and SHG mode. As indicated in Eq. (3), the more compact the A_{eff} is, the more efficient conversion we will get. Table 2 summaries the calculated A_{eff} of the present cladding waveguides from the measured mode profiles according to Eq. (4).

Optics EXPRESS

Table 2. Calculated effective interaction areas of WG1, WG2 and WG3 waveguides.

Sample	A_{eff} (μm^2)	
WG1	1368 (62.3 °C)	1167 (69.1 °C)
WG2	3069 (96.1 °C)	4978 (99.5 °C)
WG3	2361 (187.9 °C)	917 (194.3 °C)
WG4	no data	

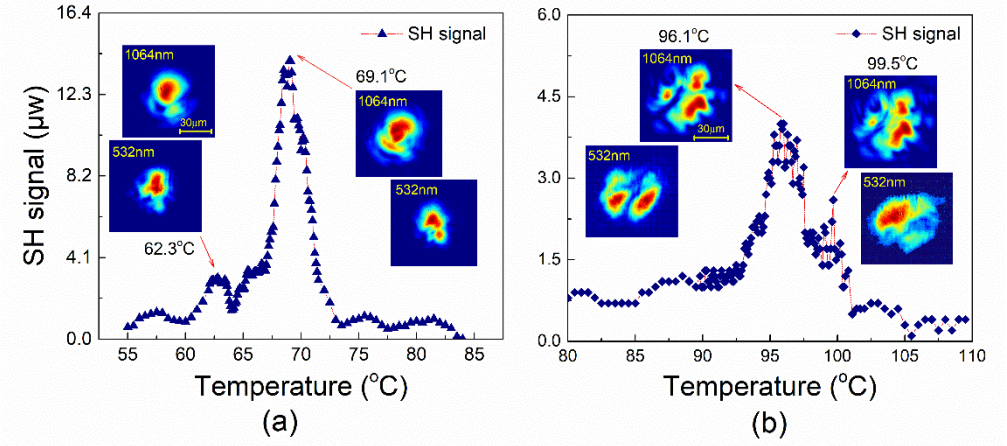

Fig. 4. (a) The temperature dependence of SHG power of WG1 waveguide. (b) The temperature dependence of SHG power of WG2 waveguide. Inset figures are the mode profiles of 1064/532nm at both QPM temperatures.

Figure 4 shows the SHG power versus the temperature of the WG1 and WG2 waveguides. Figure 4(a) is the SHG tuning curve of WG1 waveguide. Two SHG power peaks can be found in the figure which means that QPM has been realized in both temperatures. The corresponding temperatures are 62.3°C and 69.1°C, respectively. The inset figures are the mode profiles of 1064 nm (pump) and 532 nm (SHG) at two QPM points. Quasi-single mode guiding can be seen in WG1 sample under two temperatures. We also can find side node which belongs to another high order mode. Irregular mode profiles of 1064nm and 532 nm can be found at the two temperatures which are resulted by the disturbance of the excrescent focus points. As can be seen in Fig. 1(b), several tracks in WG1 and WG2 waveguides have additional break-down points on the top of the tracks. These excrescent points are the multi-foci generation sites which are induced by the self-focus/defocus phenomena inside the SLT crystal. The excrescent focus points affect the mode profile of the waveguide which can be seen in Fig. 4(a) clearly. Figure 4(b) shows the SHG curves of WG2 waveguide. The inset figures are the pump/SHG mode profiles at two peaks (96.1°C and 99.5°C). As can be seen in Fig. 4(b), the peak SHG power (4.0 μW) of WG2 is much lower than WG1 (13.9 μW). The biggest A_{eff} is found in WG2 waveguide at temperature of 99.5°C. This large area is caused by the big radius of WG2 waveguide and the asymmetry mode profiles.

Figure 5 is the tuning curve of SHG power versus the temperature of WG3 waveguide. We can find two SHG power peaks (187.9°C and 194.3°C) which satisfy the QPM conditions. The inset figures are the mode patterns of 1064/532nm at two QPM temperatures, respectively. As we can see, the pump (1064 nm) light shows single mode guiding at both peaks. For SHG light, single mode guiding is found at 194.3°C but multi-mode guiding with three nodes is found at 187.9°C. Figure 1(b) also shows the microscope picture of WG3 and WG4 waveguides. No excrescent focus points are found in the waveguide region. It has been mentioned that the scanning velocity of WG3 and WG4 is 0.75 mm/s, which is faster than that of WG1 and WG2 waveguides. As a result, the energy with lower density was absorbed along the scanning direction which cannot induce the multi foci phenomena. The absence of

the excrescent foci points enables a regular index profile which lead to symmetry mode profiles at pump/SHG wavelength. The peak power of SHG at 194.3°C is about 17.3 μW which is nearly two and a half times larger than the power at 187.9°C. The A_{eff} of both temperature points are also listed in Table 2. The A_{eff} of WG3 at 187.9°C is about 2361 μm^2, three times bigger than the A_{eff} of 917 μm^2 at 194.3°C. The bigger effective cross section at 187.9°C is induced by the excrescent modes which lead to poor overlapping with the pump mode profile.

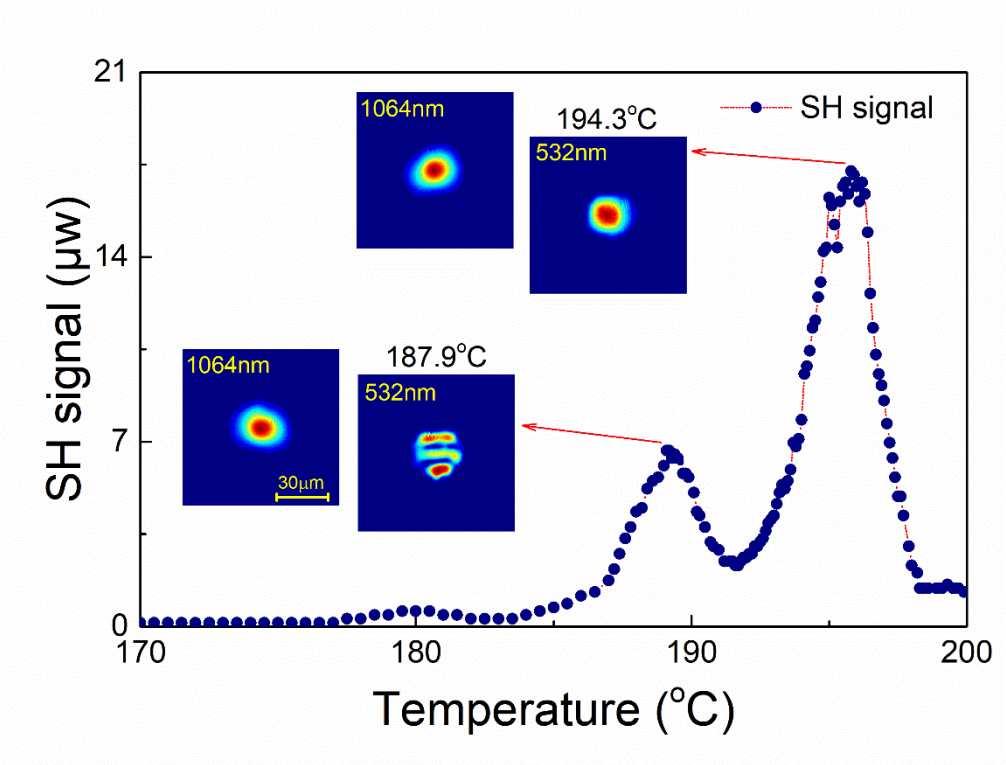

Fig. 5. The temperature dependence of SHG power of WG3 waveguide. The inset figures are the mode profiles at 1064/532nm at the QPM temperature points.

The predicted conversion efficiency of WG3 at 194.3°C is about 2.11%W^{-1}cm^{-2} by substituting the calculated A_{eff} into the right side of Eq. (3). We can also estimate the experimental conversion efficiency by the middle expression of Eq. (3). The output power of pump light before the rear face is about 79 mW, the length of WG3 waveguide is 8.9mm approximately. Therefore, the calculated conversion efficiency is about 0.74%W^{-1}cm^{-2} which is only one third of the predicted value. There are two main factors to determine the final conversion efficiency of the nonlinear waveguide device. One is the SHG ability including the d_{33} coefficient profile and the A_{eff} of the waveguide. Another is the linear propagation loss at the wavelength of the pump and SHG. In the former investigation, the SHG ability at the damage tracks was found to be eliminated due to a destruction of the crystalline structure [32]. However, strong SHG signal was found around the focal region indicating a structure inhomogeneity and drastic index perturbation. Since the guiding region of the WG3 cladding waveguides is far away from the track region we assume that the SHG ability inside our cladding waveguides remains unchanged. Note that we calculate the experimental conversion efficiency by the powers of pump/SHG light before the light output from the waveguide, the highly damped SHG light during the propagation will lead to the underestimation of the conversion efficiency. However, we cannot measure the precise propagation loss of the SHG

Optics EXPRESS

light because we found that the WG3 waveguide is multimode under wavelength of 532nm. We also note that the predicted conversion efficiency is unsatisfied. The main reason for the low conversion efficiency is the quite large A_{eff} compared to the former nonlinear waveguide devices [2–4]. Therefore, Type I/II waveguides in $LiTaO_3$ is expected due to their compact cross section.

For WG4 waveguide, no apparent SHG signal was found during the temperature tuning process from room temperature to 205°C, which is the limitation of the oven. The experimental QPM temperatures (where the highest SHG conversion occurs) of all the waveguides are listed in Table 1. The calculated values which correspond to the bulk material are also included for the comparison. It is found that the experimental QPM temperature of WG1 and WG2 waveguides are higher than the bulk values. On the other hand, the QPM temperature of WG3 waveguide are lower than the bulk. The index of the MgO doped SLT crystal increases when the temperature rises. In another words, if we assume that the effective index of WG3 waveguide mode is higher than the bulk, QPM temperature of WG3 waveguide should decrease (the effective indices of pump and SHG will decrease at the same time) compared to the bulk material in order to compensate the dispersion change of WG3 waveguide. Since both the pump and SHG light of WG3 waveguide show single mode guiding at 194.3°C, we simulated the effective indices of both wavelength by using the FD-BPM method (Rsoft BeamPROP) at different temperatures. The index contrast of WG3 was estimated by measuring the numerical aperture of the waveguide [60] and calculated with the following equation:

$$\Delta n_e \approx \frac{\sin^2 \theta_m}{2n_e} \tag{5}$$

where θ_m is the maximum incident angular deflection where no change of the transmitted power occurred, n_e is the refractive index of $LiTaO_3$. A θ_m of 5.2° was achieved which is correspond to an index contrast of 1.9×10^{-3} in the core region in WG3 waveguide. The calculated QPM periods are depicted in Fig. 2(b) (red dot line). We also note that the measured mode profiles of pump and SHG signals in WG1 and WG2 waveguides show the multimode patterns. Therefore, the dispersion behaviors are very complicated in WG1 and WG2 waveguides. A complete understanding of these phenomena needs detailed studies about the index change profile across the whole waveguide region at both 1064nm and 532nm.

4. Conclusions

In summary, nonlinear cladding waveguides in *z*-cut periodically poled $MgO:LiTaO_3$ crystal were fabricated by FLW method. The optical properties of the fabricated waveguides were analyzed. SHG via QPM process has been achieved in these FLW waveguides at wavelength of 1064 nm with aid of temperature tuning. We found that the QPM temperatures and the SHG powers of the fabricated cladding waveguides are quite different. The single mode guiding of pump light is critical to the high conversion efficiency of cladding waveguide in $MgO:LiTaO_3$. The QPM temperatures were dependent to the poling period and the features of the waveguides.

Funding

National Natural Science Foundation of China (NSFC) (61775120, 11874239); Junta de Castilla y León (Project SA046U16); Spanish Ministerio de Economía y Competitividad (MINECO, FIS2013-44174-P, FIS2015-71933-REDT).

Optics EXPRESS

References

1. S. Tanzilli, W. Tittel, H. De Riedmatten, H. Zbinden, P. Baldi, M. DeMicheli, D. B. Ostrowsky, and N. Gisin, "PPLN waveguide for quantum communication," The European Physical Journal D-Atomic, Molecular and Optical Physics **18**, 155–160 (2002).
2. K. R. Parameswaran, R. K. Route, J. R. Kurz, R. V. Roussev, M. M. Fejer, and M. Fujimura, "Highly efficient second-harmonic generation in buried waveguides formed by annealed and reverse proton exchange in periodically poled lithium niobate," Opt. Lett. **27**(3), 179–181 (2002).
3. O. Toshiharu and S. Toshiaki, "Annealed proton-exchanged waveguide quasi-phase-matched second-harmonic generation devices in 8 mol % MgO-doped congruent $LiTaO_3$ crystal," Jpn. J. Appl. Phys. **54**(10), 100304 (2015).
4. M. Lobino, M. Marangoni, R. Ramponi, E. Cianci, V. Foglietti, S. Takekawa, M. Nakamura, and K. Kitamura, "Optical-damage-free guided second-harmonic generation in 1% MgO-doped stoichiometric lithium tantalate," Opt. Lett. **31**(1), 83–85 (2006).
5. M. F. P. C. Martins Costa, R. N. Nogueira, A. A. Albuquerque, B. J. Puttnam, J. Hirohashi, M. V. Drummond, S. Shinada, R. N. Nogueira, and N. Wada, "Investigation of PPSLT waveguides for applications in optical communication systems," in Second International Conference on Applications of Optics and Photonics(2014).
6. K. Daneshvar, E. A. Giess, A. M. Bacon, D. G. Dawes, L. A. Gea, and L. A. Boatner, "Ion exchange in potassium titanyl phosphate," Appl. Phys. Lett. **71**(6), 756–758 (1997).
7. L. Ma, O. Slattery, T. Chang, and X. Tang, "Non-degenerated sequential time-bin entanglement generation using periodically poled KTP waveguide," Opt. Express **17**(18), 15799–15807 (2009).
8. F. Chen and J. R. V. Aldana, "Optical waveguides in crystalline dielectric materials produced by femtosecond-laser micromachining," Laser Photonics Rev. **8**(2), 251–275 (2014).
9. E. L. Wooten, K. M. Kissa, A. Yi-Yan, E. J. Murphy, D. A. Lafaw, P. F. Hallemeier, D. Maack, D. V. Attanasio, D. J. Fritz, G. J. McBrien, and D. E. Bossi, "A Review of Lithium Niobate Modulators for Fiber-Optic Communications Systems," IEEE J. Sel. Top. Quant. **6**(1), 69–82 (2000).
10. H. Hu, R. Ricken, and W. Sohler, "Low-loss ridge waveguides on lithium niobate fabricated by local diffusion doping with titanium," Appl. Phys. B **98**(4), 677–679 (2010).
11. R. Regener and W. Sohler, "Loss in Low-Finesse Ti: $LiNbO_3$ Optical Waveguide Resonators," Appl. Phys. B **36**(3), 143–147 (1985).
12. B. K. Das, R. Ricken, V. Quiring, H. Suche, and W. Sohler, "Distributed feedback-distributed Bragg reflector coupled cavity laser with a Ti:(Fe:)Er:$LiNbO_3$ waveguide," Opt. Lett. **29**(2), 165–167 (2004).
13. L. Wang, C. E. Haunhorst, M. F. Volk, F. Chen, and D. Kip, "Quasi-phase-matched frequency conversion in ridge waveguides fabricated by ion implantation and diamond dicing of MgO:$LiNbO_{(3)}$ crystals," Opt. Express **23**(23), 30188–30194 (2015).
14. G. B. Montanari, P. De Nicola, S. Sugliani, A. Menin, A. Parini, A. Nubile, G. Bellanca, M. Chiarini, M. Bianconi, and G. G. Bentini, "Step-index optical waveguide produced by multi-step ion implantation in $LiNbO_3$.," Opt. Express **20**(4), 4444–4453 (2012).
15. X. Liu, D. Du, and G. Mourou, "Laser ablation and micromachining with ultrashort laser pulses," IEEE J. Quantum Electron. **33**(10), 1706–1716 (1997).
16. P. P. Pronko, S. K. Dutta, J. Squier, J. V. Rudd, D. Du, and G. Mourou, "Machining of sub-micron holes using a femtosecond laser at 800 nm," Opt. Commun. **114**(1-2), 106–110 (1995).
17. J. R. Vázquez de Aldana, P. Moreno, and L. Roso, "Ultrafast lasers: A new frontier for optical materials processing," Opt. Mater. **34**(3), 572–578 (2012).
18. K. M. Davis, K. Miura, N. Sugimoto, and K. Hirao, "Writing waveguides in glass with a femtosecond laser," Opt. Lett. **21**(21), 1729–1731 (1996).
19. H. Sun, F. He, Z. Zhou, Y. Cheng, Z. Xu, K. Sugioka, and K. Midorikawa, "Fabrication of microfluidic optical waveguides on glass chips with femtosecond laser pulses," Opt. Lett. **32**(11), 1536–1538 (2007).
20. M. Ams, G. Marshall, D. Spence, and M. Withford, "Slit beam shaping method for femtosecond laser direct-write fabrication of symmetric waveguides in bulk glasses," Opt. Express **13**(15), 5676–5681 (2005).
21. Y. Liao, J. Xu, Y. Cheng, Z. Zhou, F. He, H. Sun, J. Song, X. Wang, Z. Xu, K. Sugioka, and K. Midorikawa, "Electro-optic integration of embedded electrodes and waveguides in $LiNbO_3$ using a femtosecond laser," Opt. Lett. **33**(19), 2281–2283 (2008).
22. J. Burghoff, S. Nolte, and A. Tünnermann, "Origins of waveguiding in femtosecond laser-structured $LiNbO_3$," Appl. Phys., A Mater. Sci. Process. **89**(1), 127–132 (2007).
23. J. Burghoff, C. Grebing, S. Nolte, and A. Tünnermann, "Efficient frequency doubling in femtosecond laser-written waveguides in lithium niobate," Appl. Phys. Lett. **89**(8), 081108 (2006).
24. Y. L. Lee, N. E. Yu, C. Jung, B.-A. Yu, I.-B. Sohn, S.-C. Choi, Y.-C. Noh, D.-K. Ko, W.-S. Yang, H.-M. Lee, W.-K. Kim, and H.-Y. Lee, "Second-harmonic generation in periodically poled lithium niobate waveguides fabricated by femtosecond laser pulses," Appl. Phys. Lett. **89**(17), 171103 (2006).
25. R. R. Thomson, S. Campbell, I. J. Blewett, A. K. Kar, and D. T. Reid, "Optical waveguide fabrication in z-cut lithium niobate (LiNbO3) using femtosecond pulses in the low repetition rate regime," Appl. Phys. Lett. **88**(11), 111109 (2006).
26. J. Thomas, M. Heinrich, J. Burghoff, S. Nolte, A. Ancona, and A. Tünnermann, "Femtosecond laser-written quasi-phase-matched waveguides in lithium niobate," Appl. Phys. Lett. **91**(15), 151108 (2007).

Optics EXPRESS

27. R. Osellame, M. Lobino, N. Chiodo, M. Marangoni, G. Cerullo, R. Ramponi, H. T. Bookey, R. R. Thomson, N. D. Psaila, and A. K. Kar, "Femtosecond laser writing of waveguides in periodically poled lithium niobate preserving the nonlinear coefficient," Appl. Phys. Lett. **90**(24), 241107 (2007).
28. S. Kroesen, K. Tekce, J. Imbrock, and C. Denz, "Monolithic fabrication of quasi phase-matched waveguides by femtosecond laser structuring the $\chi^{(2)}$ nonlinearity," Appl. Phys. Lett. **107**(10), 101109 (2015).
29. S. Bhardwaj, K. Mittholiya, A. Bhatnagar, R. Bernard, J. A. Dharmadhikari, D. Mathur, and A. K. Dharmadhikari, "Inscription of type I and depressed cladding waveguides in lithium niobate using a femtosecond laser," Appl. Opt. **56**(20), 5692–5697 (2017).
30. M. P. Smayev, V. V. Dorofeev, A. N. Moiseev, and A. G. Okhrimchuk, "Femtosecond laser writing of a depressed cladding single mode channel waveguide in high-purity tellurite glass," J. Non-Cryst. Solids **480**, 100–106 (2018).
31. N. Dong, Y. Tan, A. Benayas, J. V. de Aldana, D. Jaque, C. Romero, F. Chen, and Q. Lu, "Femtosecond laser writing of multifunctional optical waveguides in a Nd:YVO_4 + KTP hybrid system," Opt. Lett. **36**(6), 975–977 (2011).
32. S. L. Li, Y. K. Ye, and M. W. Wang, "Femtosecond laser written channel optical waveguide in Nd:YAG crystal," Opt. Laser Technol. **58**, 89–93 (2014).
33. C. Cheng, Y. Jia, J. R. V. de Aldana, Y. Tan, and F. Chen, "Hybrid waveguiding structure in $LiTaO_3$ crystal fabricated by direct femtosecond laser writing," Opt. Mater. **51**(1), 190–193 (2016).
34. B. McMillen, K. P. Chen, H. An, S. Fleming, V. Hartwell, and D. Snoke, "Waveguiding and nonlinear optical properties of three-dimensional waveguides in $LiTaO_3$ written by high-repetition rate ultrafast laser," Appl. Phys. Lett. **93**(11), 111106 (2008).
35. G. D. Marshall, A. Politi, J. C. F. Matthews, P. Dekker, M. Ams, M. J. Withford, and J. L. O'Brien, "Laser written waveguide photonic quantum circuits," Opt. Express **17**(15), 12546–12554 (2009).
36. L. Sansoni, F. Sciarrino, G. Vallone, P. Mataloni, A. Crespi, R. Ramponi, and R. Osellame, "Polarization entangled state measurement on a chip," Phys. Rev. Lett. **105**(20), 200503 (2010).
37. S. Kroesen, W. Horn, J. Imbrock, and C. Denz, "Electro-optical tunable waveguide embedded multiscan Bragg gratings in lithium niobate by direct femtosecond laser writing," Opt. Express **22**(19), 23339–23348 (2014).
38. W. Horn, S. Kroesen, J. Herrmann, J. Imbrock, and C. Denz, "Electro-optical tunable waveguide Bragg gratings in lithium niobate induced by femtosecond laser writing," Opt. Express **20**(24), 26922–26928 (2012).
39. Y. Tan, A. Rodenas, F. Chen, R. R. Thomson, A. K. Kar, D. Jaque, and Q. Lu, "70% slope efficiency from an ultrafast laser-written Nd:$GdVO_4$ channel waveguide laser," Opt. Express **18**(24), 24994–24999 (2010).
40. Y. Ren, G. Brown, A. Ródenas, S. Beecher, F. Chen, and A. K. Kar, "Mid-infrared waveguide lasers in rare-earth-doped YAG," Opt. Lett. **37**(16), 3339–3341 (2012).
41. H. Liu, Y. Jia, J. R. Vázquez de Aldana, D. Jaque, and F. Chen, "Femtosecond laser inscribed cladding waveguides in Nd:YAG ceramics: fabrication, fluorescence imaging and laser performance," Opt. Express **20**(17), 18620–18629 (2012).
42. E. Kifle, P. Loiko, X. Mateos, J. R. Vázquez de Aldana, A. Ródenas, U. Griebner, V. Petrov, M. Aguiló, and F. Díaz, "Femtosecond-laser-written hexagonal cladding waveguide in Tm:$KLu(WO_4)_2$: μ-Raman study and laser operation," Opt. Mater. Express **7**(12), 4258–4268 (2017).
43. E. Kifle, X. Mateos, J. R. V. de Aldana, A. Ródenas, P. Loiko, S. Y. Choi, F. Rotermund, U. Griebner, V. Petrov, M. Aguiló, and F. Díaz, "Femtosecond-laser-written Tm:KLu(WO₄)₂ waveguide lasers," Opt. Lett. **42**(6), 1169–1172 (2017).
44. X. Chen, P. Karpinski, V. Shvedov, K. Koynov, B. Wang, J. Trull, C. Cojocaru, W. Krolikowski, and Y. Sheng, "Ferroelectric domain engineering by focused infrared femtosecond pulses," Appl. Phys. Lett. **107**(14), 141102 (2015).
45. X. Chen, P. Karpinski, V. Shvedov, A. Boes, A. Mitchell, W. Krolikowski, and Y. Sheng, "Quasi-phase matching via femtosecond laser-induced domain inversion in lithium niobate waveguides," Opt. Lett. **41**(11), 2410–2413 (2016).
46. Z. D. Wei, C. Wang, H. Wang, X. Hu, D. Wei, X. Fang, Y. Zhang, D. Wu, Y. Hu, J. Li, N. S. Zhu, and M. Xiao, "Experimental demonstration of a three-dimensional lithium niobate nonlinear photonic crystal," Nat. Photonics **12**(10), 596–600 (2018).
47. T. T. Xu, K. Switkowski, X. Chen, S. Liu, K. Koynov, H. H. Yu, J. H. Zhang, J. Wang, Y. Sheng, and W. Krolikowski, "Three-dimensional nonlinear photonic crystal in ferroelectric barium calcium titanate," Nat. Photonics **12**(10), 591–595 (2018).
48. D. Sun, Y. Leng, Y. Sang, X. Kang, S. Liu, X. Qin, K. Cui, B. K. Wan Hairul Anuar, H. Liu, and Y. Bi, "Nd:MgO:$LiTaO_3$ crystal for self-doubling laser applications: growth, structure, thermal and laser properties," CrystEngComm **15**(37), 7468–7474 (2013).
49. M. Nakamura, S. Takekawa, K. Terabe, K. Kitamura, T. Usami, K. Nakamura, H. Ito, and Y. Furukawa, "Near-Stoichiometric $LiTaO_3$ for Bulk Quasi-Phase-Matched Devices," Ferroelectrics **273**(1), 199–204 (2002).
50. J. P. Meyn and M. M. Fejer, "Tunable ultraviolet radiation by second-harmonic generation in periodically poled lithium tantalate," Opt. Lett. **22**(16), 1214–1216 (1997).
51. T. Hatanaka, K. Nakamura, T. Taniuchi, H. Ito, Y. Furukawa, and K. Kitamura, "Quasi-phase-matched optical parametric oscillation with periodically poled stoichiometric $LiTaO_{(3)}$," Opt. Lett. **25**(9), 651–653 (2000).
52. A. Bruner, D. Eger, and S. Ruschin, "Second-harmonic generation of green light in periodically poled stoichiometric $LiTaO_3$ doped with MgO," J. Appl. Phys. **96**(12), 7445–7449 (2004).

Optics EXPRESS

53. Y. Nan Ei, O. Myoung-Kyu, K. Hoonsoo, J. Changsoo, K. Bok Hyeon, L. Kyu-Sup, K. Do-Kyeong, T. Shunji, and K. Kenji, "Continuous tuning of a narrow-band terahertz wave in periodically poled stoichiometric $LiTaO_3$ crystal with a fan-out grating structure," Appl. Phys. Express **7**(1), 012101 (2014).
54. X. P. Hu, P. Xu, and S. N. Zhu, "Engineered quasi-phase-matching for laser techniques," Photon. Res. **1**(4), 171–185 (2013).
55. Y. Ishigame, T. Suhara, and H. Nishihara, "$LiNbO_{(3)}$ waveguide second-harmonic-generation device phase matched with a fan-out domain-inverted grating," Opt. Lett. **16**(6), 375–377 (1991).
56. A. Bruner, D. Eger, M. B. Oron, P. Blau, M. Katz, and S. Ruschin, "Temperature-dependent Sellmeier equation for the refractive index of stoichiometric lithium tantalate," Opt. Lett. **28**(3), 194–196 (2003).
57. H. H. Lim, S. Kurimura, T. Katagai, and I. Shoji, "Temperature-Dependent Sellmeier Equation for Refractive Index of 1.0mol% Mg-Doped Stoichiometric Lithium Tantalate," Jpn. J. Appl. Phys. **52**(3), 032601 (2013).
58. A. C. Muir, G. J. Daniell, C. P. Please, I. T. Wellington, S. Mailis, and R. W. Eason, "Modelling the formation of optical waveguides produced in $LiNbO_3$ by laser induced thermal diffusion of lithium ions," Appl. Phys., A Mater. Sci. Process. **83**(3), 389–396 (2006).
59. S. Mailis, C. Riziotis, I. T. Wellington, P. G. R. Smith, C. B. E. Gawith, and R. W. Eason, "Direct ultraviolet writing of channel waveguides in congruent lithium niobate single crystals," Opt. Lett. **28**(16), 1433–1435 (2003).
60. Y. Yao, Y. Tan, N. Dong, F. Chen, and A. A. Bettiol, "Continuous wave Nd:YAG channel waveguide laser produced by focused proton beam writing," Opt. Express **18**(24), 24516–24521 (2010).